# NONLINEAR LUMPED CIRCUIT MODEL OF GaAs MESFET

by

L. O. Chua and Y. W. Sing

Memorandum No. UCB/ERL M82/73

19 October 1982

# NONLINEAR LUMPED CIRCUIT MODEL OF GaAs MESFET

by

L. O. Chua and Y. W. Sing

Memorandum No. UCB/ERL M82/73

19 October 1982

ELECTRONICS RESEARCH LABORATORY

College of Engineering
University of California, Berkeley
94720

# Nonlinear Lumped Circuit Model of GaAs MESFET[†]

by

L. O. Chua and Y. W. Sing[††]

Department of Electrical Engineering and Computer Sciences
and the Electronics Research Laboratory
University of California, Berkeley, California 94720

## Abstract

A nonlinear lumped circuit model for GaAs MESFET which includes the effect of Gunn-domain formation under the gate, mobility modulation, and diffusion process in the channel boundary is presented. The important design parameters such as $C_{in}$, $g_m$, $I_{dsat}$ and $F_t$ etc. can be derived from the model. The model not only predicts realistically the nonlinear I-V characteristics, but it also provides a closed form design criterion for avoiding instability due to Gunn oscillation. Moreover, a small-signal circuit model having the same basic circuit structure as the existing empirical small-signal model in [2,10,14] can be derived from this nonlinear model.

In addition, a two-segment piecewise-linear DC model is derived. This piecewise-linear model contains only four model parameters which can be determined very easily by measurement. Because of its simplicity, this model can be implemented into any CAD system to simulate complex circuits with significantly less CPU time. The simulation results are in excellent agreement with experimental data, and with results obtained by a much more time-consuming two-dimensional calculation.

---

[†]Research supported by the Office of Naval Research under Contract N00014-76-C-0572.

[††]L.O. Chua and Y.W. Sing are with the Department of EECS, University of California, Berkeley.

## I. INTRODUCTION

GaAs MESFET is a three-terminal Gunn effect device with a Schottky control gate. Because of its high-gain, high-speed and low-noise property, GaAs MESFET has become increasingly important in both microwave and high-speed digital circuits.

Two-dimensional analysis shows that: 1) The mobile carrier distribution is not abrupt at the depletion layer boundary as in the gradual channel approximation [1,2]. In other words, a transition region exists in the depletion boundary and its width is close to the effective channel thickness of the modern GaAs MESFET structure. 2) Field-dependent mobility causes a reduction of the drain current [9]. 3) The formation of a stationary Gunn domain at the drain side of the gate is responsible for the current saturation in GaAs MESFET [2,3,9].

Several GaAs MESFET lumped circuit models have been proposed over the past decade. The Schottky model [12] has been developed for general JFET analysis purposes, but none of the above important effects has been included. The Lettovec and Zuleeg model [3] takes into consideration the mobility-field dependence, but does not consider the decrease in drift-velocity with increasing field due to Gunn effect. It therefore can not simulate the saturation region correctly. The Engelman and Liechti model [6] takes into consideration both Gunn-domain formation and mobility modulation effect. However, it is only a semi-empirical model and is not derived from device physics. The Shur model [9,11] uses the standard Schottky theory while adding a Gunn domain to achieve a reasonably good agreement. However, it is only a small-signal model and therefore can not simulate the nonlinear characteristics. Finally, we remark that none of the above models takes into consideration the important fact that the boundary between the neutral and depleted

regions of the channel is not abrupt, and that also none of the existing small-signal models [9,10,11,13] is derived as a special case of a realistic nonlinear model.

Our objective in this paper is to present a new nonlinear lumped circuit model which not only considers all the important effects mentioned above, but also does not require any iteration in calculating the DC characteristics. Also, a small-signal model is derived from this nonlinear model, which agrees with existing empirical small-signal models [13] for microwave operations.

In addition, a two-segment piecewise-linear DC model is derived. This model contains only 4 model parameters which not only can be easily determined by measurement, but also have physical meanings. Because of its simplicity, this model is particularly useful for implementation in CAD systems to simulate complex GaAs circuits, such as high-speed GaAs LSI circuits. Simulation results are in good agreement with both two-dimensional calculations and experimental data.

## II. DESCRIPTION OF THE NONLINEAR MODEL

Our nonlinear lumped circuit model, which will be derived and evaluated in section VI, is shown in Fig. 1(a) along with its circuit symbol and small-signal equivalent circuit in Fig. 1(b) and Fig. 1(c), respectively. The element parameters and characteristics of the model are defined as follows:

(1). Nonlinear controlled current source $I_{ch}$:

$I_{ch}$ corresponds to the conduction current component in the channel and is defined as follow:

$$I_{ch} = \frac{G_0}{1+\frac{LV_1}{E_c}} \left\{ aV_1 - \frac{2}{3}\left[(V_1+V_b-V_{gs}-b)^{3/2} - (V_b-V_{gs}-b)^{3/2}\right] \right\}$$
$$\triangleq I_{ch}(V_1, V_{gs}) \qquad (1)$$

where

$$G_0 = \frac{W}{L} U_0 Q N_o d$$

$$a = 1 - (0.5 - U_r)\left(\frac{\Delta}{d}\right)$$

$$b = \frac{1}{12}\left(\frac{\Delta}{k}\right)^2$$

$$\Delta = \left(\frac{2}{\pi}\right) c L_d$$

$$L_d = \sqrt{\frac{\varepsilon K_0 T}{Q^2 N_0}}$$

$$k = \sqrt{\frac{2\varepsilon}{Q N_0}}$$

$d$ is the channel thickness (typical value: 0.1 μm to 1 μm)

$W$ is the channel width (typical value: 0.5 μm to 1000 μm)

$L$ is the channel length (typical value: 0.5 μm to 10 μm)

$Q$ is the electron charge ($1.6 \times 10^{-19}$ Coulomb)

$N_0$ is the channel doping (typical value: $1 \times 10^{15} cm^{-3}$ to $5 \times 10^{17} cm^{-3}$)

$U_0$ is the low-field electron mobility (typical value: 4.5 K to 8.0 K $cm^2/V.sec$)

$E_c$ is the critical field (typical value: 3.5 K to 6.0 K V/cm)

$V_b$ is the built-in potential (typical value: 0.5 to 0.8 volt)

$c$ is a proximity factor, (typical value: 6)

$U_r$ is ratio of effective mobility in the transition region to the low-field mobility (typical value: 0.2 to 0.5)

(2). Nonlinear control current source $I_{do}$:

$I_{do}$ corresponds to the conduction current in the Gunn domain and is defined as follows:

$$I_{do} = I_a - C_d F(V_1, V_2, V_{gs}) \triangleq I_{do}(V_1, V_2, I_a, V_{gs}) \qquad (2)$$

where $I_a$ is labelled in Fig. 1(c), $C_d$ is defined in (5), and $F(V_1,V_2,V_{gs})$ is defined as follows:

$$F(V_1,V_2,V_{gs}) = \int_{E_1}^{E_1+k\sqrt{V_2}} [v(E_1) - v(E)]dE \tag{3}$$

where v(E) denotes the field-dependent electron drift velocity, $E_1$ denotes the electric field intensity of the channel under the drain end of the gate and is defined as follows:

$$E_1 = \frac{I_{ch}(V_1,V_{gs})}{G_0L[a - \frac{k}{d}\sqrt{V_1+V_b-V_{gs}}-b] - \frac{I_{ch}(V_1,V_{gs})}{E_c}} \tag{4}$$

Since $I_{do}$ depends on $V_1$, $V_2$, $I_a$, and $V_{gs}$, we denote it by $I_{do}(V_1,V_2,I_a,V_{gs})$ in Fig. 1(a).

(3). Domain Capacitance:

$$C_d = \frac{\varepsilon A}{W_d} \tag{5}$$

where

$W_d$ = average domain width

$$= \lim_{T\to\infty} \frac{1}{T} \int_0^T X_{dom}(t)dt \tag{6}$$

where $X_{dom}(\cdot)$ is a nonlinear function related to the domain width as defined in [7].

(4). Nonlinear gate capacitance:

$$C_{gd} = \frac{C_{gd0}}{\sqrt{1 - \frac{V_{gd}}{V_b}}} \tag{7a}$$

$$C_{ga} = \frac{C_{ga0}}{\sqrt{1 - \frac{V_{ga}}{V_b}}} \tag{7b}$$

$$C_{gs} = \frac{C_{gso}}{\sqrt{1 - \frac{V_{gs}}{V_b}}} \tag{7c}$$

where

$C_{gd0}$, $C_{ga0}$, and $C_{gs0}$ are zero-bias capacitances, and $V_b$ is the built-in potential.

(5). Nonlinear voltage-controlled current source:

$$I_{gd} = I_{gds}\, e^{(V_{gd}/V_t)} \tag{8a}$$

$$I_{ga} = I_{gas}\, e^{(V_{ga}/V_t)} \tag{8b}$$

$$I_{gs} = I_{gss}\, e^{(V_{gs}/V_t)} \tag{8c}$$

where

$I_{gds}$, $I_{gas}$ and $I_{gss}$ are ideal saturation currents for the Schottky junctions, and $V_t$ is the thermal voltage (26 mV at 300°K)

## III. DESCRIPTION OF PIECEWISE-LINEAR MODEL AND PARAMETER DETERMINATION METHOD

Although the nonlinear GaAs MESFET model presented in section II is useful in predicting the complex nonlinear dynamic behaviors of the device, it is still inefficient for large circuits. Moreover, it is rather time-consuming to determine the model parameters. In the GaAs MESFET LSI development, it is necessary to have a simple yet reasonably accurate model to be used in such computer-aided circuit

analysis programs as SPICE, MSINC, ASPEC, etc., in order to simulate circuits containing a large number of circuit elements. Two-dimensional analysis is accurate but too expensive to be implemented in circuit simulation programs and is only good for device development purposes. On the other hand, the conventional junction FET model which does not consider velocity saturation caused by the Gunn-domain formation, can not give a reasonably accurate simulation.

In this section, we will present a simple piecewise-linear model which is derived from the more accurate nonlinear model in section II. Inspite of its simplicity, the piecewise-linear model not only takes into account the velocity saturation effect caused by the Gunn-domain formation, but also the source and drain resistance effects. Because of its simplicity, this model can be implemented into any CAD system to simulate complex circuits requiring a significantly less CPU time.

This piecewise-linear model, which will be derived in section VI, is described as follows:

Piecewise-Linear Model

For $V_{ds} < V_{dsat}$,

$$I_{ds} = \frac{B[\sqrt{V_b-V_p} - \sqrt{V_b-V_{gs}}]V_{ds}}{1+R_{sd}B[\sqrt{V_b-V_p} - \sqrt{V_b-V_{gs}}]} \triangleq I_{ds}(V_{gs},V_{ds}) \qquad (9a)$$

For $V_{ds} > V_{dsat}$,

$$I_{ds} = B[\sqrt{V_b-V_p} - \sqrt{V_b-V_{gs}}]\, V_s \triangleq I_{dsat} \qquad (9b)$$

where

$V_b$ is the built-in voltage $\approx$ 0.7 volt

$$V_{dsat} = V_s[1 + R_{sd}B(\sqrt{V_b-V_p} - \sqrt{V_b-V_{gs}})] \triangleq V_{dsat}(V_{gs}) \qquad (9c)$$

Note that this model contains only four model parameters; namely,

$B$ = intrinsic transconductance

$V_p$ = pinch-off voltage

$R_{sd}$ = source and drain resistance

$V_s$ = intrinsic saturation voltage corresponding to the saturation velocity due to the Gunn domain formation.

Without knowing the detailed process and geometrical parameters, these model parameters can be determined by measurement very easily. Two examples will be given to illustrate the parameter determination method and to demonstrate the accuracy of this model.

The parameter measurement procedure is as follows:

Step 1: plot $I_{ds}$ versus $\sqrt{V_b - V_{gs}}$ in the saturation region.

Step 2: use linear regression method to obtain a straight line which best fits the data. Calculate the slope $S_1$, and the X-axis intersection $X_1$.

Step 3: plot $V_{dsat}$ versus $\sqrt{V_b - V_{gs}}$, where $V_{dsat}$ is defined as the corner voltage between the linear region and the saturation region in the $I_{ds}$ versus $V_{ds}$ characteristic.

Step 4: use linear regression method to obtain a straight line which best fits the data. Calculate the slope $S_2$.

Based on the data obtained from the above procedure, the parameters can be calculated as follows:

Piecewise-Linear Model Parameters

$$V_p = -X_1^2 + V_b$$

$$V_s = V_{dsat} \text{ at } V_{gs} = V_p$$

$$B = S_1/V_s$$

$$R_{sd} = S_2/S_1$$

Two samples from different vendors (one from TI, the other from HP) have been characterized and the model parameters obtained by the above procedure are as follows:

| TI device: | HP device: |
|---|---|
| $B = 0.202$ | $B = 0.253$ |
| $V_s = 0.48$ | $V_s = 0.31$ |
| $V_p = -4.59$ | $V_p = 1.43$ |
| $R_{sd} = 6.88$ | $R_{sd} = 11.6$ |

Two families of $I_{ds}$ vs. $V_{ds}$ characteristics are shown in Fig. 2(a) for the TI device, and in Fig. 2(b) for the HP device. The dash curves are obtained by measurement, whereas the solid curves are calculated using the piecewise-linear model. Note the remarkable agreement everywhere except near the knees where a slight discrepancy occurs.

In contrast, note the curve corresponding to $V_{gs} = 0$ calculated using the conventional Junction FET model is way off the measured curve.

## IV. NONLINEAR MODEL VALIDATION

The $I_{ds}$ versus $V_{ds}$ characteristics for GaAs MESFET (with $d = 0.4$ μm and $N_0 = 3\times10^{16}cm^{-3}$) as obtained by a two-dimensional simulation [2] are shown in Fig. 3(a). Using the same parameters in the nonlinear model in Fig. 1(a), we calculated the characteristics (drawn with small circles) shown in Fig. 3(a). Although our model requires a much less computation time, the agreement is very good. Note that the $I_{ds}$ versus $V_{ds}$ characteristics in Fig. 3(a) exhibit the well-known "negative resistance" behavior of the Gunn domain [7], which has been observed in highly homogeneous samples when the doping density is relatively small [2].

In Fig. 3(b) the active channel capacitance is calculated using the nonlinear GaAs MESFET model in Fig. 1(a) and compared to the experimental data [14]. The agreement is good over the entire operating range. The initially decreasing value of $C_{in}$ is due to the increase in the depletion width. The active channel capacitance $C_{in}$ approaches its minimum at a value of $V_{ds}$ where the high-field domain is formed. By further increasing $V_{ds}$, $C_{in}$ increases monotonically. This phenomenon is attributed to the Gunn-domain formation in the channel.

The transconductance $g_m$ and the cut-off frequency $F_t$ are calculated using the nonlinear GaAs MESFET model in Fig. 1(a) and compared to the experimental data in Figs. 3(c) and 3(d), respectively. Note that both $g_m$ and $F_t$ decrease monotonically for values of $V_{ds}$ greater than $V_{dsat}$. This phenomenon is again attributed to Gunn-domain formation in the channel.

## V. GUNN OSCILLATION CRITERION

Depending on the device's physical and geometrical parameters, and bias conditions, the GaAs MESFET can be operated at different modes; namely Gunn oscillation, stable negative resistance, and normal FET modes. Therefore, it is important to establish the criterion of instability which results from the Gunn effect. In this section, we will present a closed form Gunn-oscillation criterion for GaAs MESFET.

A Gunn domain starts to form when $E_1$ reaches the threshold field $E_p$. If the electric field intensity in the drain side ohmic region is greater than the domain sustaining field $E_s$, the domain will travel from the drain end of the gate to the drain contact and causes instability. Thus a Gunn-oscillation criteria can be derived using this observation.

Since the current in the drain side ohmic region must be equal to the channel current, the electric-field intensity in the drain side ohmic region $E_0$ can be related to $E_1$ as follows:

$$E_0 = \frac{E_1}{1+\frac{E_1}{E_c}} \left[1 - \frac{k}{d}\left(\sqrt{V_1+V_b-V_{gs}-b}\right)\right] \tag{10}$$

Thus, the stability criterion is given by

$$E_s < \frac{E_p}{1+\frac{E_p}{E_c}} \left[1 - \frac{k}{d}\left(\sqrt{V_1+V_b-V_{gs}-b}\right)\right] \tag{11}$$

## VI. DERIVATION OF THE MODEL

### A. Assumptions

The nonlinear GaAs MESFET model in section II is based on the following assumptions:

1. The conduction current in the channel is dominated by majority carriers (neglect the minority carriers) [1].
2. Due to the diffusion process, the boundary between the neutral and the depleted portions of the channel is not abrupt. In other words, a transition region exists in the order of several Debye lengths. Also the carrier concentration changes gradually in this transition region [1,2], and the distribution is approximated by a linear junction.
3. The mobility modulation effect causes a reduction of the drain current [3].
4. The formation of a stationary Gunn domain at the drain side of the gate is responsible for the current saturation [2,4,5,6,9]. The high-

field domain will form when the maximum electric field intensity under the gate reaches the electron peak velocity field $E_p$ [4,5]. After the high-field domain has been formed, the relation between the domain voltage $V_2$ and the electric field intensity $E_1$ at the drain side of the channel can be determined by a one-dimensional model [2,4]. The description of the Gunn-domain characteristic is based on the result developed in [7].

5. The ohmic resistance of the channel-to-source and the channel-to-drain portions of the device are assumed to be in series with the channel and the Gunn domain. They can be modeled realistically by linear resistors [2] and treated as external components connected to the "intrinsic" nonlinear model in Fig. 1(a).

B. Derivation of the Nonlinear Model

Consider the two-dimensional GaAs MESFET structure as shown in Fig. 4(a) along with its symbol in Fig. 4(b). If we apply a reverse bias gate voltage $V_{gs}$ across the device, the mobile carriers will be depleted from the metal-semiconductor junction, leaving the depletion layer as shown in Fig. 5. Two-dimensional numerical analysis [1,2] shows that the boundary between the neutral and the depleted portions of the channel is not abrupt. Generally, the formula describing the transition region is very complicated and has to be solved by two-dimensional algorithms [1]. For simplicity, the mobile carriers in the transition region are assumed to be a linear function of y, where y denotes the vertical distance indicated in Fig. 5. The electron density distribution is expressed as follows:

1) In the completely neutral region:

$$\text{for } 0 < y < t, \quad N = N_0 \tag{12a}$$

where t and N denote the thickness and electron concentration in the neutral region.

2) In the transition region:

$$\text{for } t < y < t+\Delta, \quad N = N_0\left(1 - \frac{y-t}{\Delta}\right) \tag{12b}$$

where

$\Delta = \left(\frac{2}{\pi}\right) cL_d$

$L_d$ is the Debye length ($L_d = \sqrt{\epsilon K_0 T/Q^2 N_0}$),

c is the proximity factor which has been estimated from two-dimensional analysis [1] to be equal to 6 [1].

3) In the completely depleted region:

$$\text{for } t+\Delta < y < d, \quad N = 0 \tag{12c}$$

where

d is the channel thickness.

Figure 6 shows the piecewise-linear approximation of the electron density distribution used in this paper, as well as the one used in the two-dimensional analysis in [1,2]. The result shows that the piecewise-linear approximation is reasonably accurate.

By using Poisson's equation with Eqs. (12a), (12b) and (12c), the following voltage across the junction can be obtained:

$$V_{gx} = \frac{QN_0}{2\epsilon}\left[\frac{1}{3}\Delta^2 + (d-t)(d-t-\Delta)\right] \tag{13}$$

The thickness t in the complete neutral region is given by:

$$t = d - \frac{\Delta}{2} - \sqrt{\frac{2\epsilon}{QN_0} V_{gx} - \frac{1}{12}\Delta^2} \tag{14}$$

Note that if no transition region is assumed, Eq. (14) agrees with the result calculated from the one-dimensional one-sided abrupt junction

approximation. The conduction current in the channel is given by

$$I_{ch}(x) = W \int_0^d N(x,y)\ v(x,y)dy \tag{15}$$

where

W is the channel width.

N(x,y) is the mobile charge density.

v(x,y) is the electron velocity.

d is the channel thickness.

Substituting Eqs. (12a), (12b), (12c), and (14) into (15), we obtained:

$$I_{ch}(x) = WdQN_0\left\{\left[1 - \frac{\Delta}{2d} - \frac{k}{d}\sqrt{V_{gx} - \frac{1}{12}\left(\frac{\Delta}{k}\right)^2}\right] V(x,y) + \int_t^{t+\Delta}\left(1 - \frac{y-t}{\Delta}\right)V(x,y)dy\right\}$$

$$= WdQN_0U\left\{\left[1 - \frac{\Delta}{2d} - \frac{k}{d}\sqrt{V_{gx} - \frac{1}{12}\left(\frac{\Delta}{k}\right)^2}\right]E_x + \frac{\Delta}{d}V_{eff}\right\} \tag{16}$$

where

V(x,y) denotes the carrier velocity

$$V_{eff} = \frac{1}{\Delta}\int_t^{t+} \left(1 - \frac{y-t}{\Delta}\right)V_x(x,y)dy \tag{17}$$

$$V_x(x,y) = \frac{V(x,y)E_x}{\sqrt{Ex^2+Ey^2}} \tag{18}$$

The characteristic of $V_{eff}$ versus $E_x$ is calculated and is shown in Fig. 7. For simplicity, we can introduce a proximity factor $U_r$ such that,

$$V_{eff} = U_rV(x,y) = U_rU_0E_x \tag{19}$$

Substituting Eq. (19) into Eq. (16), we obtain

$$I_{ch}(x) = WdQN_0U[1 - \frac{\Delta}{d}(\frac{1}{2} - U_r) - \frac{k}{d}\sqrt{V_{gx} - \frac{1}{12}(\frac{\Delta}{k})^2}]E_x$$

$$= WdQN_0U[a - \frac{k}{d}\sqrt{V_{gx}-b}]E_x \tag{20}$$

where

$$a = 1 - (\frac{\Delta}{d})(\frac{1}{2} - U_r) \tag{21}$$

and

$$b = \frac{1}{12}(\frac{\Delta}{k})^2 \tag{22}$$

Also it was shown in [3] that the drain current is reduced due to the mobility modulated by the field in the x-direction. In order to incorporate this effect, the following empirical expression given in [1,3] is used for the mobility U in the channel region:

$$U = \frac{U_0 E_x}{1 + \frac{E_x}{E_c}} \tag{23}$$

where $U_0$ denotes the low-field mobility, and $E_c$ denotes the critical field.

Since the electric field under the gate is always smaller than the electron-velocity peak field, Eq. (23) is a reasonally good approximation for the relation between velocity and electric field in the channel region. Substituting Eq. (23) into Eq. (20), we obtain the conduction current in the channel:

$$I_{ch}(x) = \frac{WQN_0dU_0}{1 + \frac{E_x}{E_c}}\left[ a - \frac{k}{d}\sqrt{V_{gx} - \frac{1}{12}(\frac{\Delta}{k})^2} \right] E_x \tag{24}$$

Simplifying Eq. (24), we obtain

$$I_{ch}(x) = \frac{WQN_0dU_0}{1 + \frac{dv}{dx}/E_c}\left[a - \frac{k}{d}\sqrt{V_{gx} - \frac{1}{12}(\frac{\Delta}{k})^2}\right]\frac{dv}{dx} \tag{25}$$

Integrating both sides of Eq. (25) over the channel region, we obtained,

$$I_{ch} = \frac{G_0}{1+\frac{LV_1}{E_c}} \left\{ aV_1 - \frac{2}{3}\frac{k}{d}\left[(V_1+V_b-V_{gs}-b)^{3/2} - (V_b-V_{gs}-b)^{3/2}\right]\right\} \tag{26}$$

Note that if we set $\Delta = 0$, in Eq. (26), (i.e., no transition region) and $E_c = \infty$, (i.e., no mobility modulation by x-direction field), then Eq. (26) simplifies to the classic Schottky expression in the linear region.

Now let us consider the conduction current under the drain end of the gate

$$I_a = \frac{G_0 L}{1+\frac{E_1}{E_c}} \left[a - \frac{k}{d}\sqrt{V_1+V_b-V_{gs}-b}\right] E_1 \tag{27}$$

Since the current at any point in the channel must be equal, $I_{ch}(V_1)$ is equal to $I_a$, we can equate Eqs. (26) and (27) to obtain:

$$E_1 = \frac{I_{ch}(V_1,V_{gs})}{G_0 L\left[a - \frac{k}{d}\sqrt{V_1+V_b-V_{gs}-b}\right] - \frac{I_{ch}(V_1,V_{gs})}{E_c}} \tag{28}$$

It was shown in [4,5] that when $E_1$ exceeds the threshold field $E_p$, the Gunn domain appears and grows with increasing drain bias. We assume that the stationary Gunn domain is in series with the channel and the relation between the domain voltage $V_2$ and $E_1$ can be determined by a one-dimensional model [2]. Our description of the Gunn domain is based on the model developed in [7]. The domain voltage can be expressed as follows:

$$\frac{dV_2}{dt} = \int_{E_1}^{E_1+k\sqrt{V_2}} [v(E_1) - v(E)]dE$$

$$= g(E_1, V_2) \tag{29}$$

The gate-to-channel portion is modeled by 3 Schottky diodes whose characteristics are governed by the well-known relationships given in Eqs. 7(a), (b), (c), and Eqs. 8(a), (b), and (c), respectively. The nonlinear circuit model described by Eqs. (7), (8), (26), (28), and (29) is shown in Fig. 1(a).

C. Derivation of the Piecewise-Linear Model

Now let us derive the piecewise-linear model described in section III. For typical parameters, the voltage $V_1$ across the channel is less than $V_b - V_{gs}$. Therefore, expanding the term $[V_1 + V_b - V_{gs} - b]^{3/2}$ in Eq. (26) and neglecting higher-order terms, we obtain the following simplified expression:

$$I_{ch} = B[\sqrt{V_b - V_p} - \sqrt{V_b - V_{gs}}]\, V_1 \tag{30}$$

where

$$B = G_0 k/d$$

$$V_p = -(ad/k)^2 + V_b$$

$$V_1 = V_{ds} - I_{ch} R_{sd}$$

Substituting $V_1 = V_{ds} - I_{ch} R_{sd}$ into Eq. (30), we obtain

$$I_{ch} = \frac{B[\sqrt{V_b - V_p} - \sqrt{V_b - V_{gs}}]V_{ds}}{1 + BR_{sd}[\sqrt{V_b - V_p} - \sqrt{V_b - V_{gs}}]} \tag{31}$$

Equation (31) is valid until the Gunn domain is formed. It was shown in [2,6,8,9] that the electron velocity is saturated when the Gunn domain is formed and that the voltage across the channel under this condition is equal to $LE_s$. Hence, with $V_1 = LE_s$, Eq. (30) becomes:

$$I_{ch} = B[\sqrt{V_b - V_p} - \sqrt{V_b - V_{gs}}]\, V_s \tag{32}$$

where we introduce the new model parameter $V_s = LE_s$.

## D. Derivation of the Small-Signal Model

The preceding analysis completes our derivation of the piecewise-linear model described in section III. Let us turn next to the derivation of the small-signal circuit model. From the nonlinear model, we carry out a standard small-signal analysis by writing the following two node equations for Fig. 1(a):†

$$i_g = C_{gs} \frac{dv_{gs}}{dt} + C_{ga} \frac{dv_{ga}}{dt} + C_{gd} \frac{dv_{gd}}{dt} \tag{33}$$

$$i_{ch} = i_a + C_{ga} \frac{dv_{ga}}{dt} \tag{34}$$

From Eq. (26), we obtain,

$$\begin{aligned} i_{ch} &= g_m v_{gs} + g_i v_1 \\ &= g_m v_{ga} + (g_i + g_m) v_1 \end{aligned} \tag{35}$$

where

$$\begin{aligned} g_m &\triangleq \frac{\partial I_{ch}}{\partial V_{gs}} \\ &= \frac{G_0 k}{d} [\sqrt{V_1 + V_b - V_{gs} - b} - \sqrt{V_b - V_{gs} - b}] \end{aligned} \tag{36}$$

†All small-signal variables and parameters are denoted by lower case letters.

$$g_i \triangleq \frac{\partial I_{ch}}{\partial V_1}$$

$$= G_0[a - \frac{k}{d}\sqrt{V_1+V_b-V_{gs}-b}] \tag{37}$$

From Eq. (27), we obtain,

$$i_a = g_i e_1 + m v_{ga} \tag{38a}$$

where

$$m \triangleq \frac{\partial I_a}{\partial V_{ga}}$$

$$= \frac{-G_0 E_1 k}{2d\sqrt{V_1+V_b-V_{gs}-b}} \tag{38b}$$

From Eq. (29), we obtain,

$$(\frac{dv_2}{dt}) = ne_1 + hv_2 \tag{39}$$

where

$$n \triangleq \frac{\partial g}{\partial E_1} \tag{40}$$

$$h \triangleq \frac{\partial g}{\partial V_2} \tag{41}$$

Substituting Eq. (35), (38a), (39) into (34), we obtain,

$$(g_i+g_m)v_1 = (\frac{g_i}{n})(\frac{dv_2}{dt}) - (\frac{g_i h}{n})v_2 + C_{ga}\frac{dv_{ga}}{dt} + (m-g_m)v_{ga} \tag{42}$$

In the microwave operating range, the term $(m-g_m)v_{ga}$ is very much smaller than the other terms and can be neglected. Consequently, Eq. (42) becomes,

$$\frac{v_1}{R_i} = C_d(\frac{dv_2}{dt}) + \frac{v_2}{R_d} + C_{ga}(\frac{dv_{ga}}{dt}) \tag{43}$$

where

$$R_i \triangleq \frac{1}{g_i+g_m}$$

$$C_d \triangleq \frac{g_i}{n}$$

$$R_d \triangleq \frac{-n}{g_i h}$$

A small-signal circuit model which is described by Eqs. (33), (35), and (43) is shown in Fig. 2(c). Note that the small-signal model derived in this section is similar to the existing empirical small-signal model given in [2,10,14].

## VII. CONCLUSION

A nonlinear lumped circuit model of GaAs MESFET is proposed. The model takes into account the modulation, the Gunn-domain formation, and the diffusion process in the depletion boundary. A small-signal circuit model is derived from this nonlinear model. The structure of this small-signal circuit model is very similar to the existing empirical small-signal models currently used in microwave circuit design. In addition, a piecewise-linear model is derived. This model contains only four parameters which can be determined by measurement without knowing the detailed manufacturing process and geometrical parameters. The calculated results agree very well with those obtained by two-dimensional simulations and experimental measurements.


## Acknowledgement

The authors would like to thank Mr. Tom J. Viola from Hewlett-Packard Company for supplying several GaAs MESFET samples used in this research.

## REFERENCES


[1] Ken Yamaguchi and Hiroschi Kodera, "Drain conductance of junction gate FET's in the hot electron range," IEEE Trans. on Electron Devices, Vol. ED-23, No. 6, June 1979, pp. 1283-1290.

[2] Michael S. Shur and Lester F. Eastman, "Current-voltage characteristics, small-signal, parameters, and switching time of GaAs FET's," IEEE Trans. on Electron Devices, Vol. ED-25, No. 6, June 1978, pp. 606-611.

[3] K. Lettovec and R. Zuleeg, "Voltage-current characteristics of GaAs J-FET's in the hot electron range," Solid-State Electronics, Vol. 13, pp. 1415-1426.

[4] K. Yamaguchi and H. Kodera, "Two-dimensional numerical analysis of stability criteria of GaAs FET's," IEEE Trans. on Electron Devices, Vol. ED-23, December 1976, pp. 1283-1290.

[5] B. Himsworth, "A two-dimensional analysis of gallium arsenide junction field effect transistor with long and short channels," Solid State Electronics, Vol. 15, 1972, pp. 1353-1361.

[6] R. Engelmann and C. Liechti, "Gunn-domain formation in the saturated current region of GaAs MESFETs," IEDM Tech. Dig., December 1976, pp. 351-354.

[7] L. O. Chua and Y. W. Sing, "A nonlinear lumped circuit model for Gunn diode," International Journal of Circuit Theory and Applications, Vol. 6, December 1978, pp. 375-408.

[8] B. L. Gelmont and M. S. Shur, "Analytical theory of stable domain in high doped Gunn diodes," Electronic Letter, Vol. 6, No. 12, 1970, pp. 385-397.

[9] Michael S. Shur, "Analytical model of GaAs MESFET," IEEE Trans. Electron Devices, Vol. ED-25, No. 6, June 1978, pp. 612-618.

[10] H. Willing, "A technique for predicting large-signal performance of a GaAs MESFET," IEEE Trans. on Microwave Theory and Techniques, Vol. MTT-26, No. 12, December 1978, pp. 1017-1022.

[11] M. S. Shur, "Small-signal nonlinear circuit model of GaAs MESFET," Solid State Electronics, Vol. 22, 1979, pp. 723-728.

[12] A. S. Grove, Physics and Technology of Semiconductor Devices, Wiley, 1967.

[13] C. A. Liechti, "Microwave field-effect transistor," IEEE Trans. on Microwave Theory and Technique, Vol. MTT-24, No. 6, June 1976, pp. 279-299.

[14] R. H. Engelmann and C. A. Liechti, "Bias dependence of GaAs and InP MESFET parameters," IEEE Trans. on Electron Devices," Vol. ED-24, No. 11, November 1977, pp. 1288-1296.

LIST OF FIGURE CAPTIONS

Fig. 1. (a) GaAs MESFET nonlinear lumped circuit model.
The diamond shape symbols denote nonlinear current sources.
The symbols $V_{gs}$ and $V_{ds}$ denote the voltage from the gate to the source, and from the drain to the source, respectively.

(b) GaAs MESFET circuit symbol.

(c) GaAs MESFET small-signal circuit model.

Fig. 2. Characteristics calculated by piecewise-linear model:

(a) Texas instrument fabricated device [10].

(b) Hewelett-Packard fabricated device (HFET 1000).

Fig. 3. Comparison between measured and calculated results:

(a) Drain current versus voltage characteristics.

(b) Active channel capacitance versus voltage characteristic.

(c) Transconductance versus voltage characteristic.

(d) Cutoff frequency versus voltage characteristic.

Fig. 4. (a) GaAs MESFET cross section.

(b) GaAs MESFET circuit symbol.

Fig. 5. The channel cross section of GaAs MESFET.

Fig. 6. Comparison of electron density distribution.

Fig. 7. Effective carrier velocity in x-direction versus the electric field characteristic.

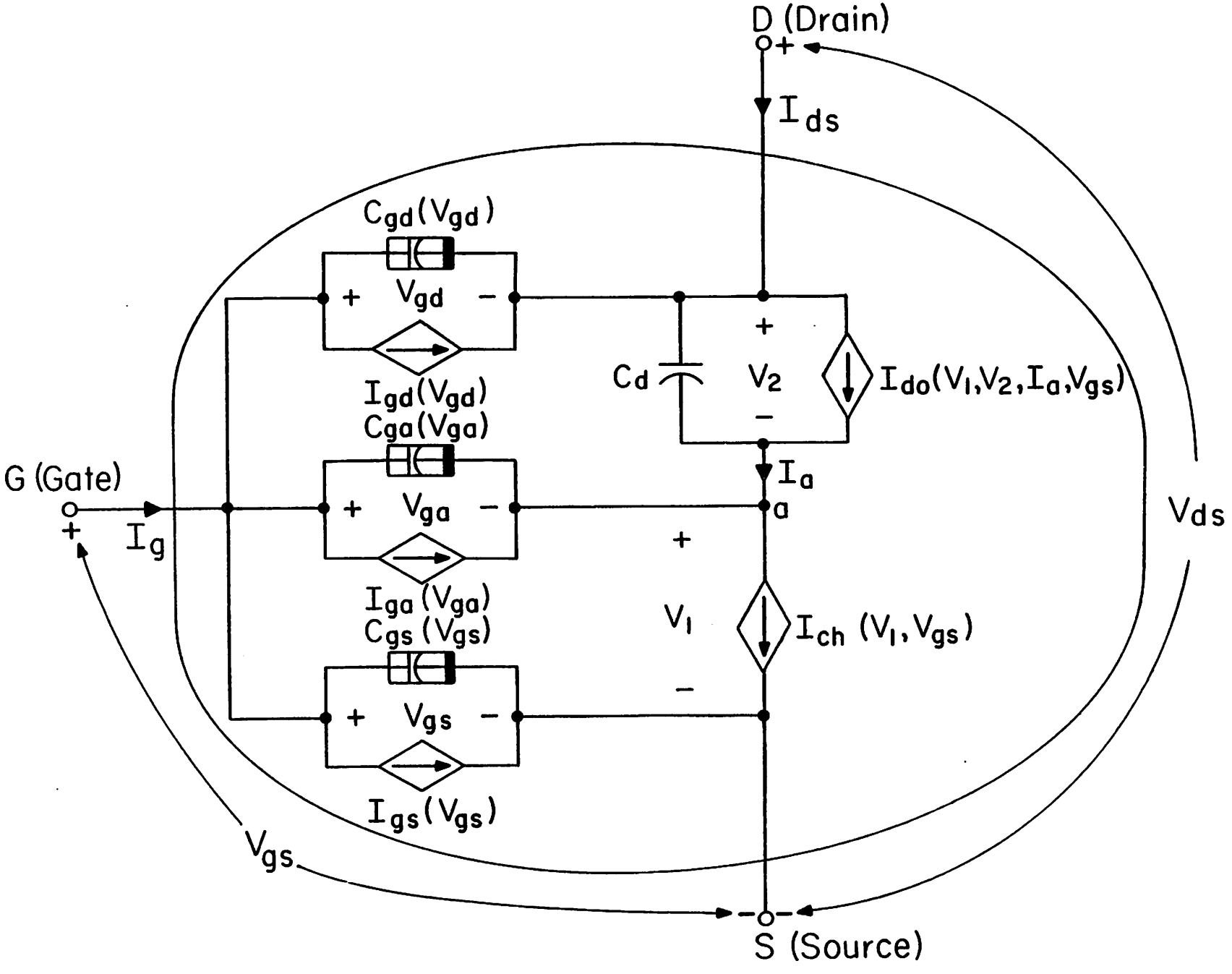
D (Drain)
+
$I_{ds}$
$C_{gd}(V_{gd})$
+ $V_{gd}$ −
$I_{gd}(V_{gd})$
$C_d$
+
$V_2$
−
$I_{do}(V_1,V_2,I_a,V_{gs})$
$C_{ga}(V_{ga})$
$I_a$
G (Gate)
+
$I_g$
+ $V_{ga}$ −
a
$V_{ds}$
+
$I_{ga}(V_{ga})$
$C_{gs}(V_{gs})$
$V_1$
$I_{ch}(V_1,V_{gs})$
−
+ $V_{gs}$ −
$I_{gs}(V_{gs})$
$V_{gs}$
−
S (Source)

Fig. 1(a)

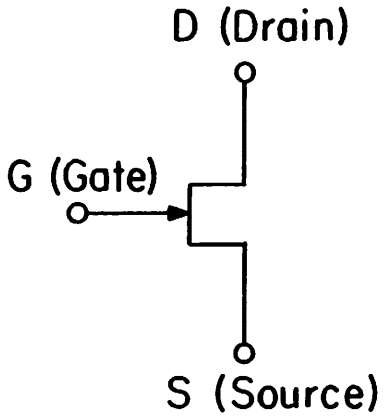
D (Drain)
G (Gate)
S (Source)

Fig. 1(b)

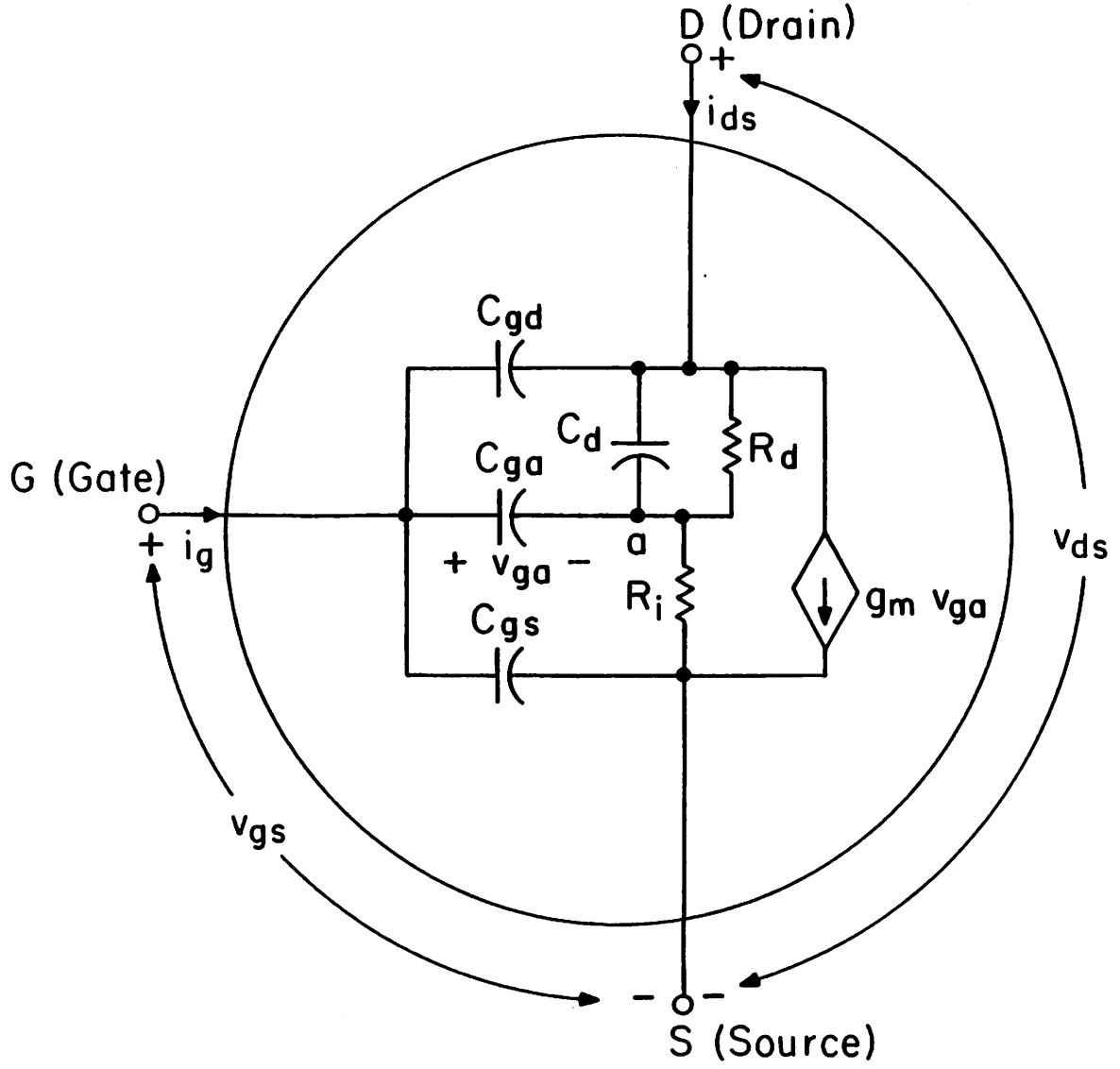
D (Drain)
+
ids
Cgd
Cd
Rd
Cga
G (Gate)
+ ig
+ vga −
a
Ri
gm vga
Cgs
vds
vgs
−
−
S (Source)

Fig. 1(c)

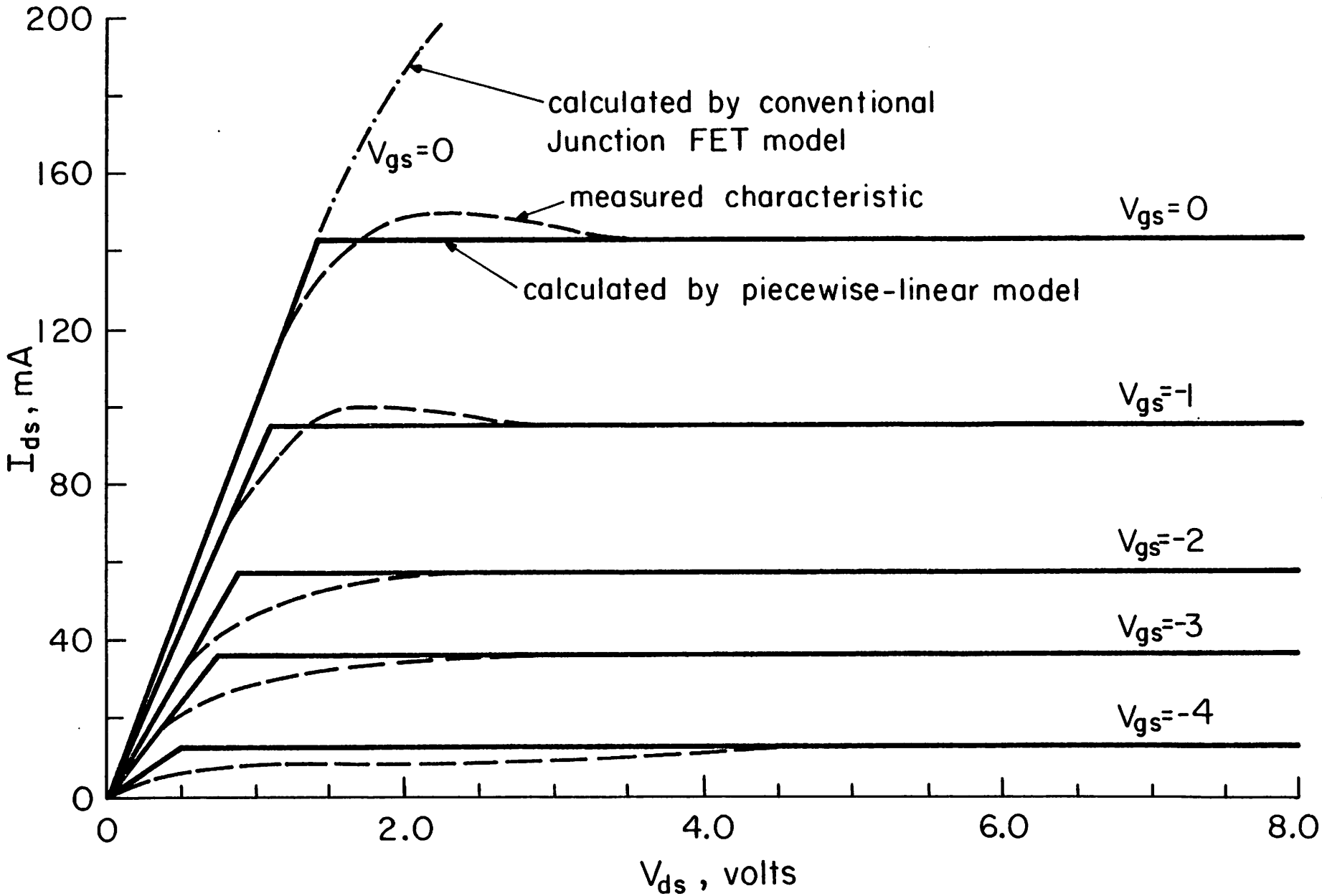
200
160
120
80
40
0
$I_{ds}$, mA
0
2.0
4.0
6.0
8.0
$V_{ds}$, volts
calculated by conventional
Junction FET model
$V_{gs}$=0
measured characteristic
$V_{gs}$=0
calculated by piecewise-linear model
$V_{gs}$=-1
$V_{gs}$=-2
$V_{gs}$=-3
$V_{gs}$=-4

Fig. 2(a)

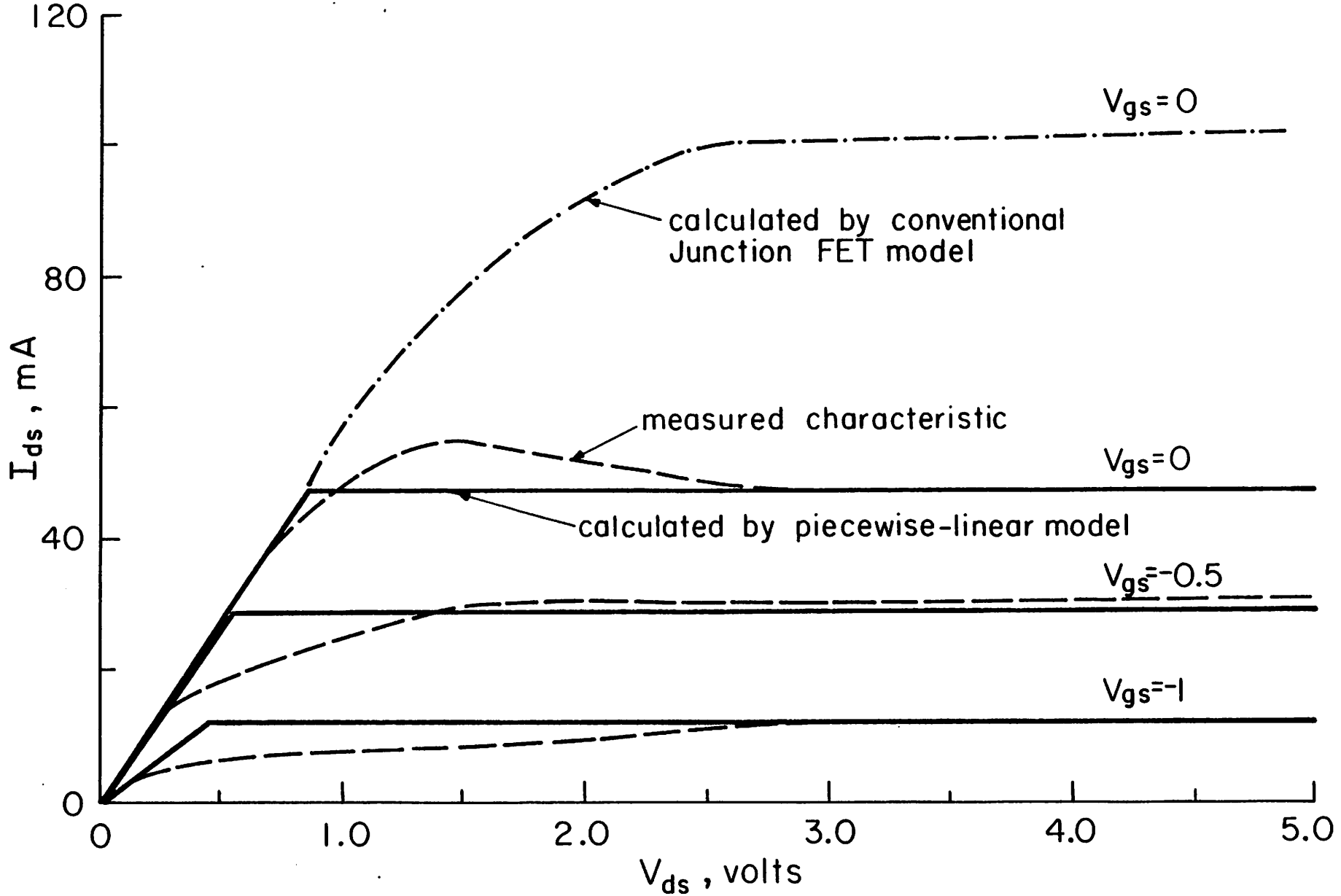
120
80
40
0
$I_{ds}$ , mA
$V_{gs}=0$
calculated by conventional
Junction FET model
measured characteristic
$V_{gs}=0$
calculated by piecewise-linear model
$V_{gs}=-0.5$
$V_{gs}=-1$
0
1.0
2.0
3.0
4.0
5.0
$V_{ds}$ , volts

Fig. 2(b)

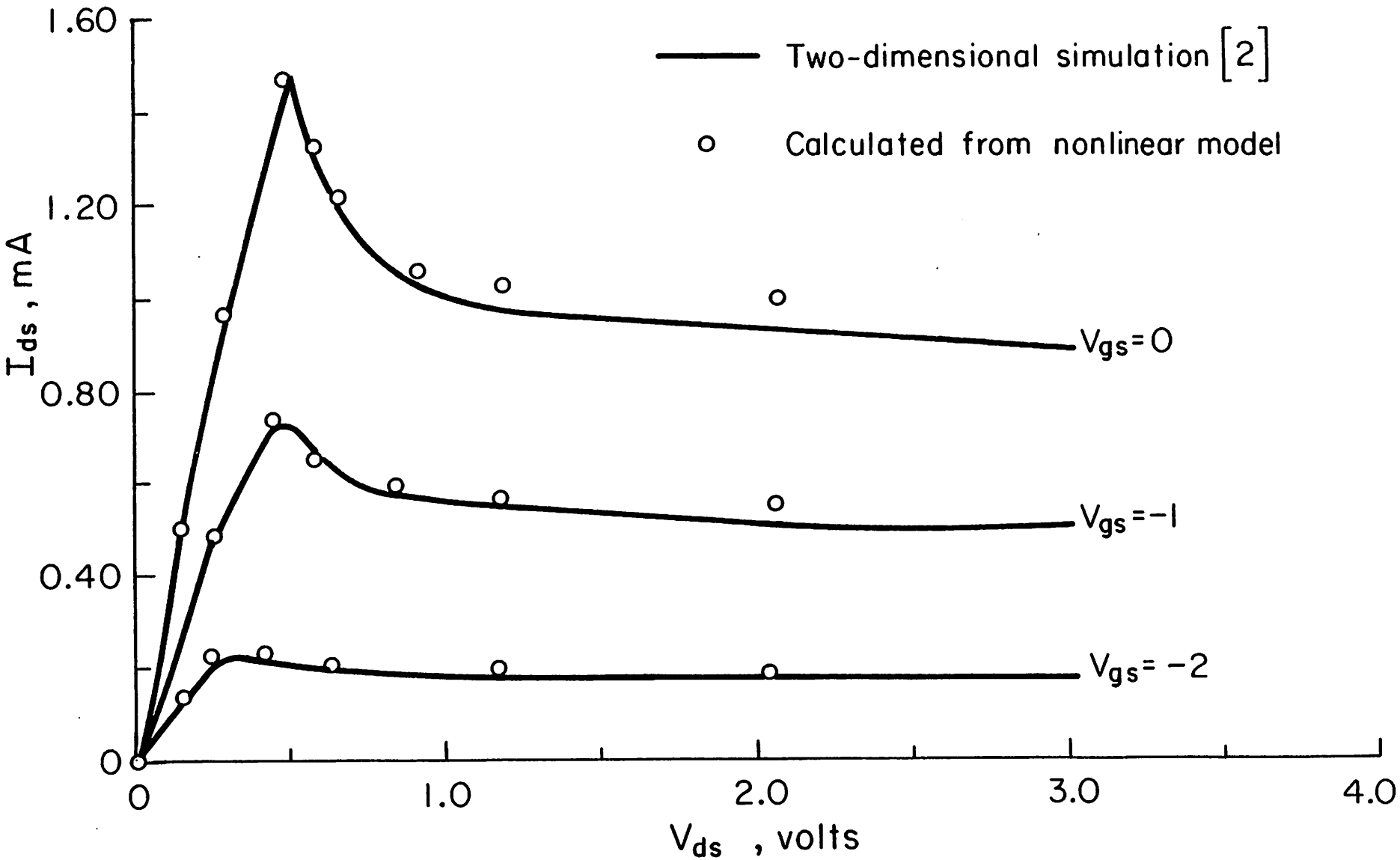
1.60
1.20
0.80
0.40
0
$I_{ds}$, mA
Two-dimensional simulation [2]
Calculated from nonlinear model
$V_{gs}$=0
$V_{gs}$=-1
$V_{gs}$=-2
0
1.0
2.0
3.0
4.0
$V_{ds}$, volts

Fig. 3(a)

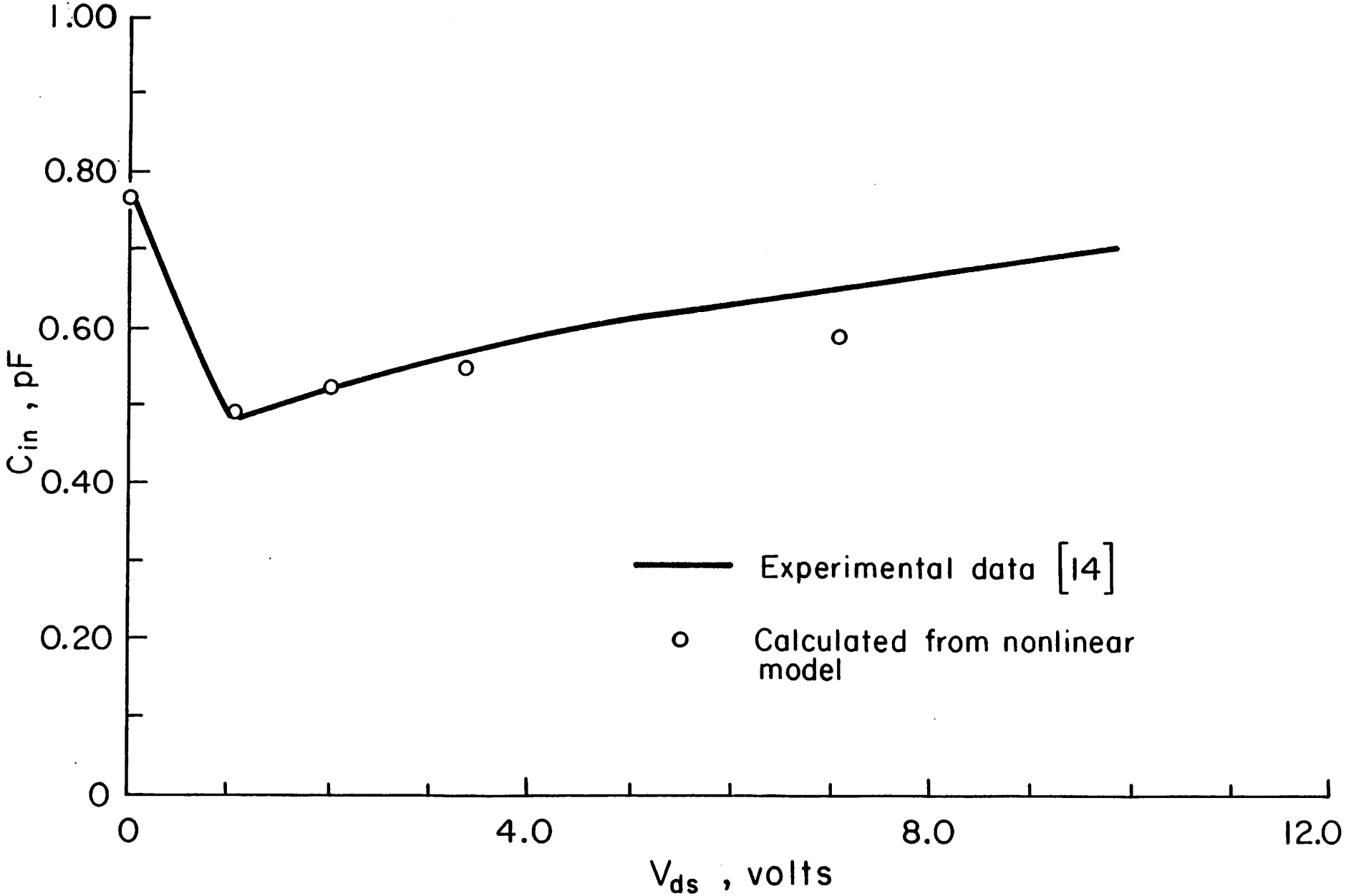
1.00
0.80
0.60
0.40
0.20
0
$C_{in}$ , pF
0
4.0
8.0
12.0
$V_{ds}$ , volts
Experimental data [14]
Calculated from nonlinear model

Fig. 3(b)

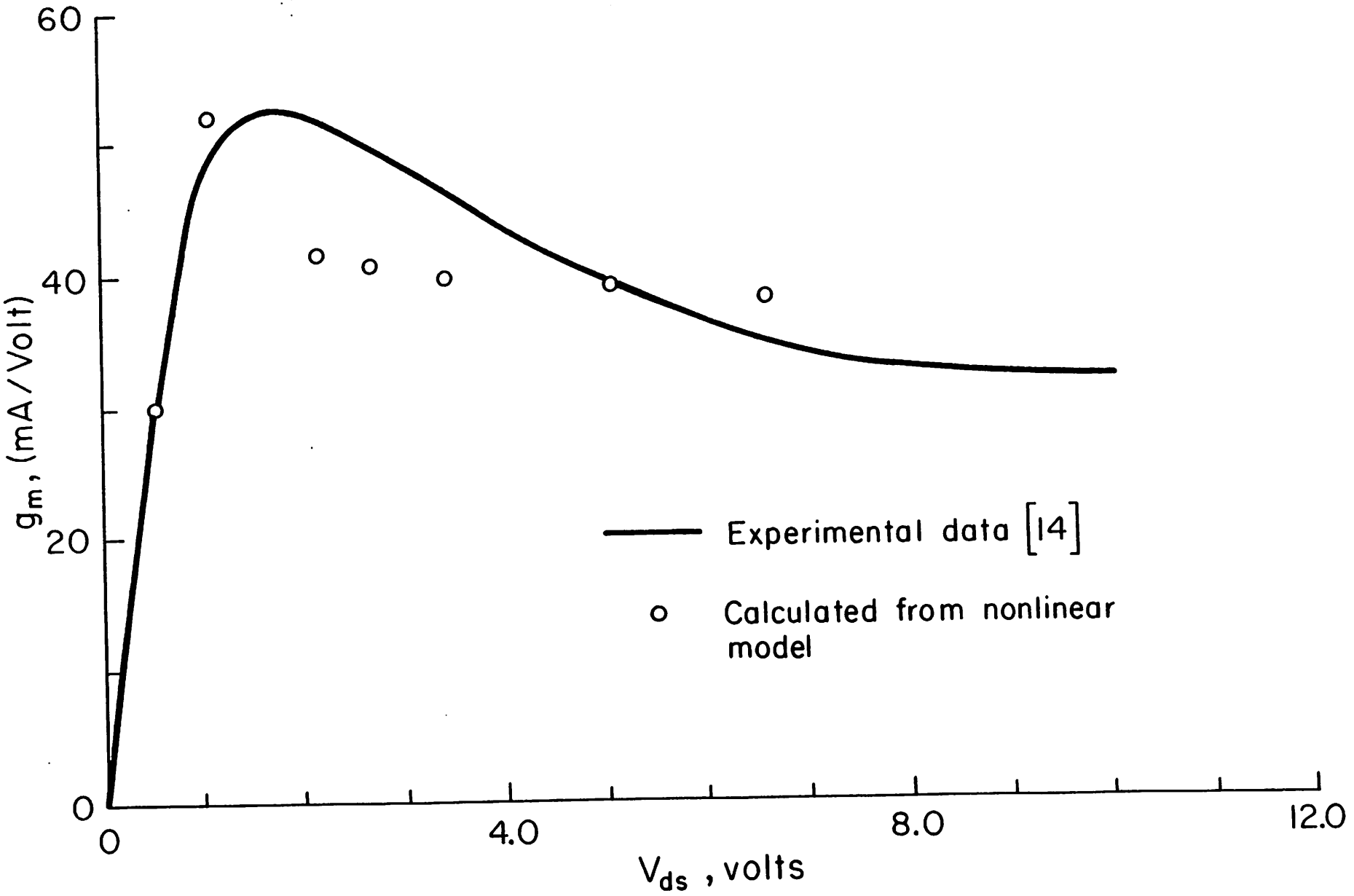
60
40
20
0
$g_m$, (mA / Volt)
0
4.0
8.0
12.0
$V_{ds}$ , volts
Experimental data [14]
Calculated from nonlinear model

Fig. 3(c)

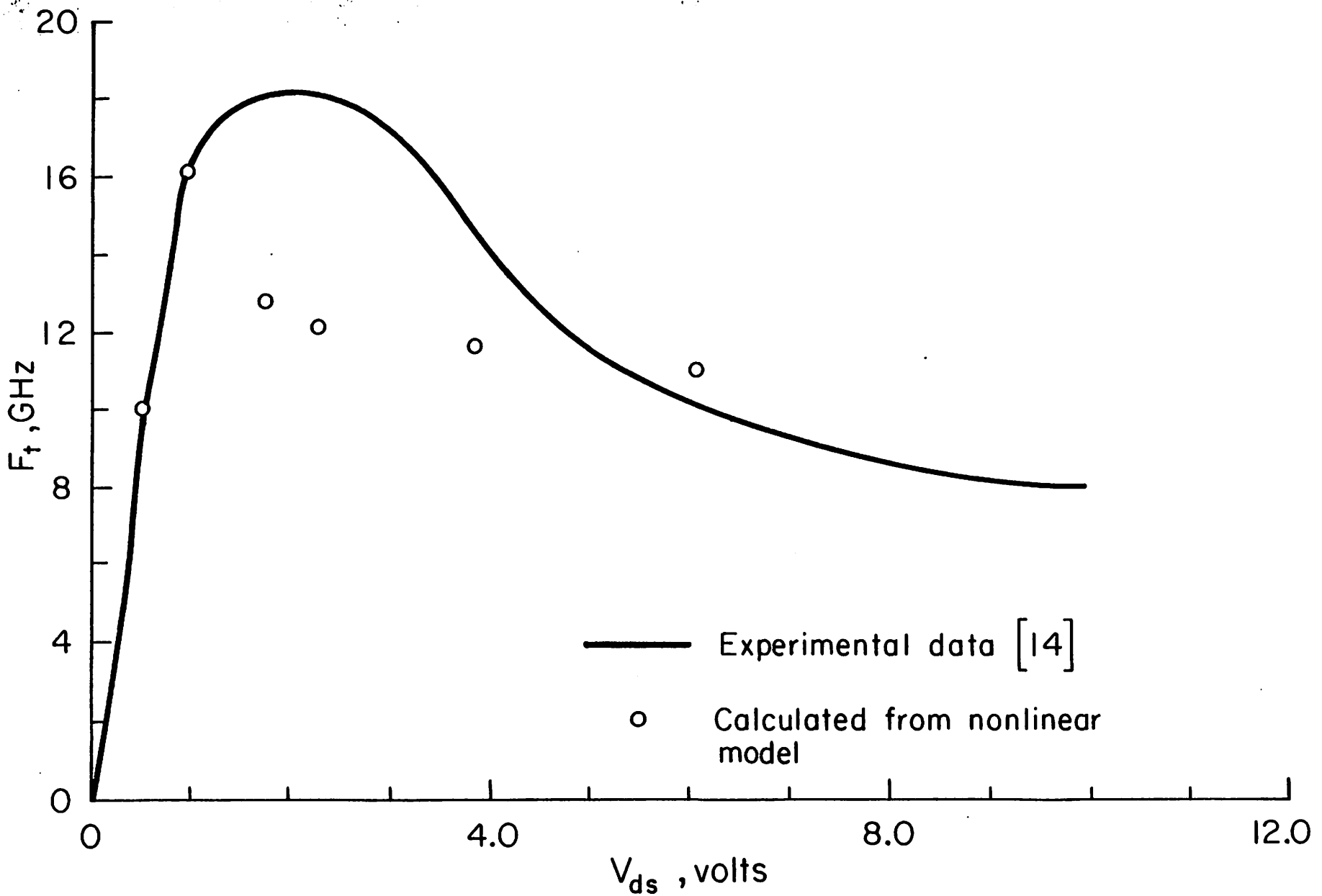
20
16
12
8
4
0
$F_t$, GHz
0
4.0
8.0
12.0
$V_{ds}$, volts
Experimental data [14]
Calculated from nonlinear model

Fig. 3(d)

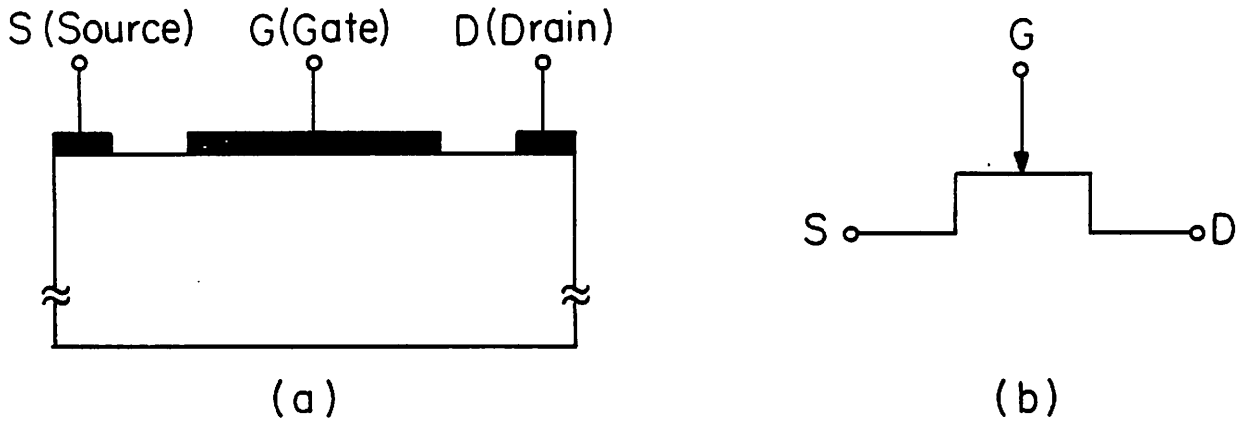
S (Source)
G(Gate)
D(Drain)
(a)
G
S
D
(b)

Fig. 4

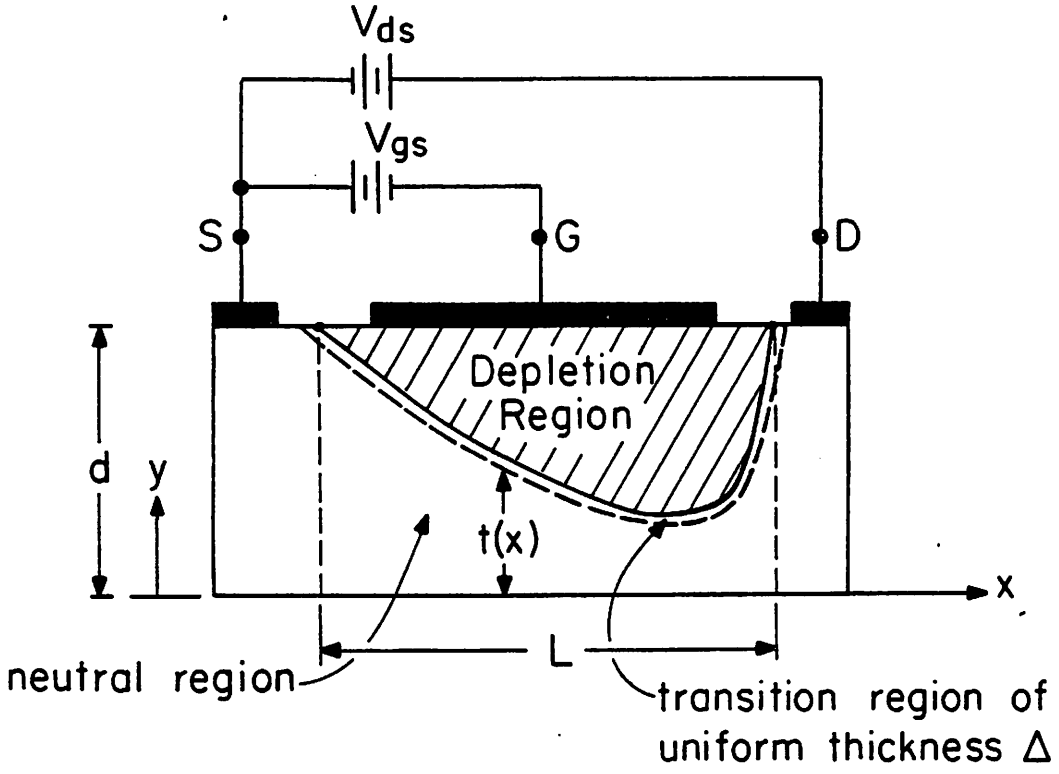
Vds
Vgs
S
G
D
Depletion Region
d
y
t(x)
x
L
neutral region
transition region of uniform thickness Δ

Fig. 5

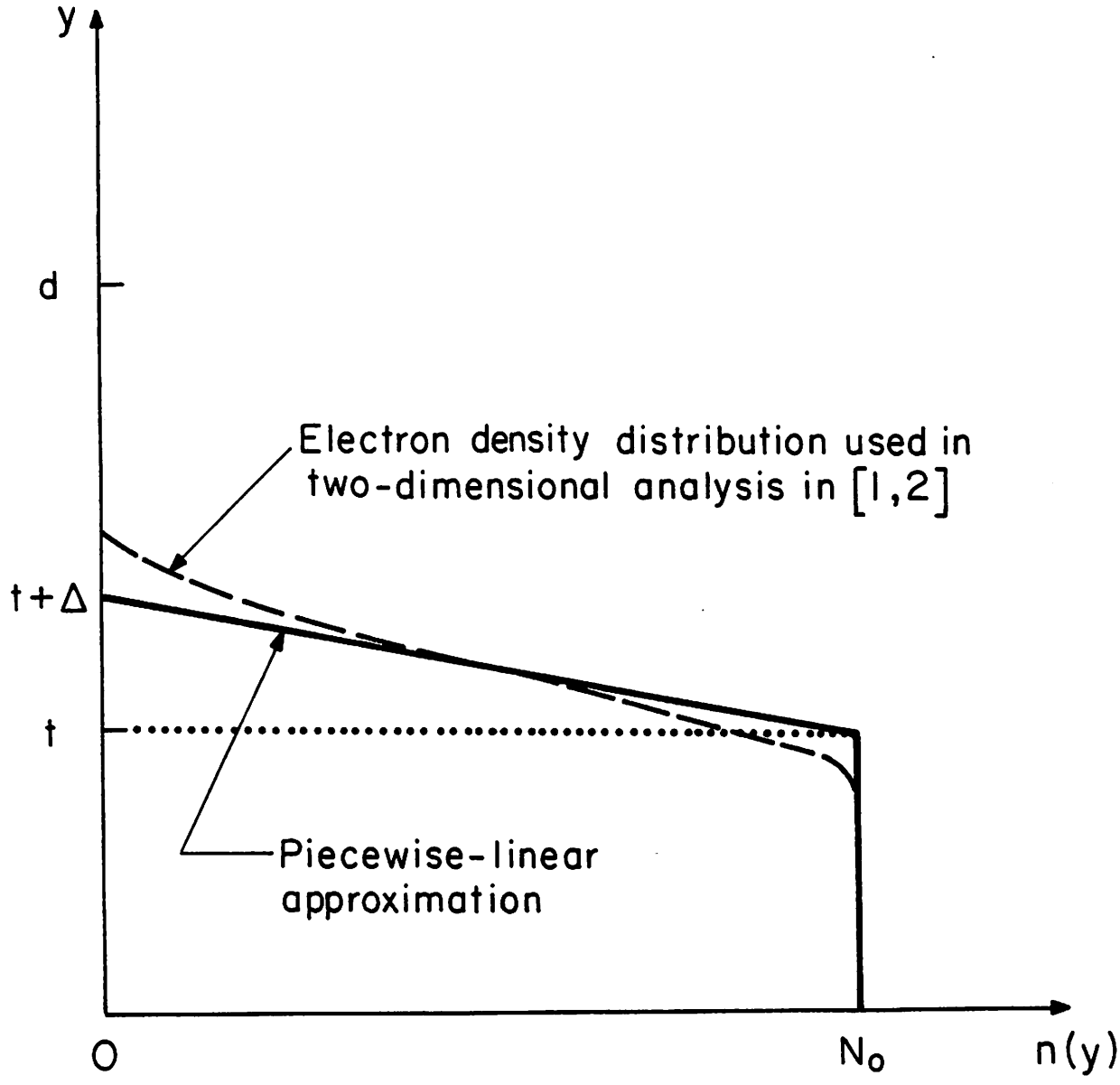
y
d
Electron density distribution used in
two-dimensional analysis in [1,2]
t+Δ
t
Piecewise-linear
approximation
0
N₀
n(y)

Fig. 6

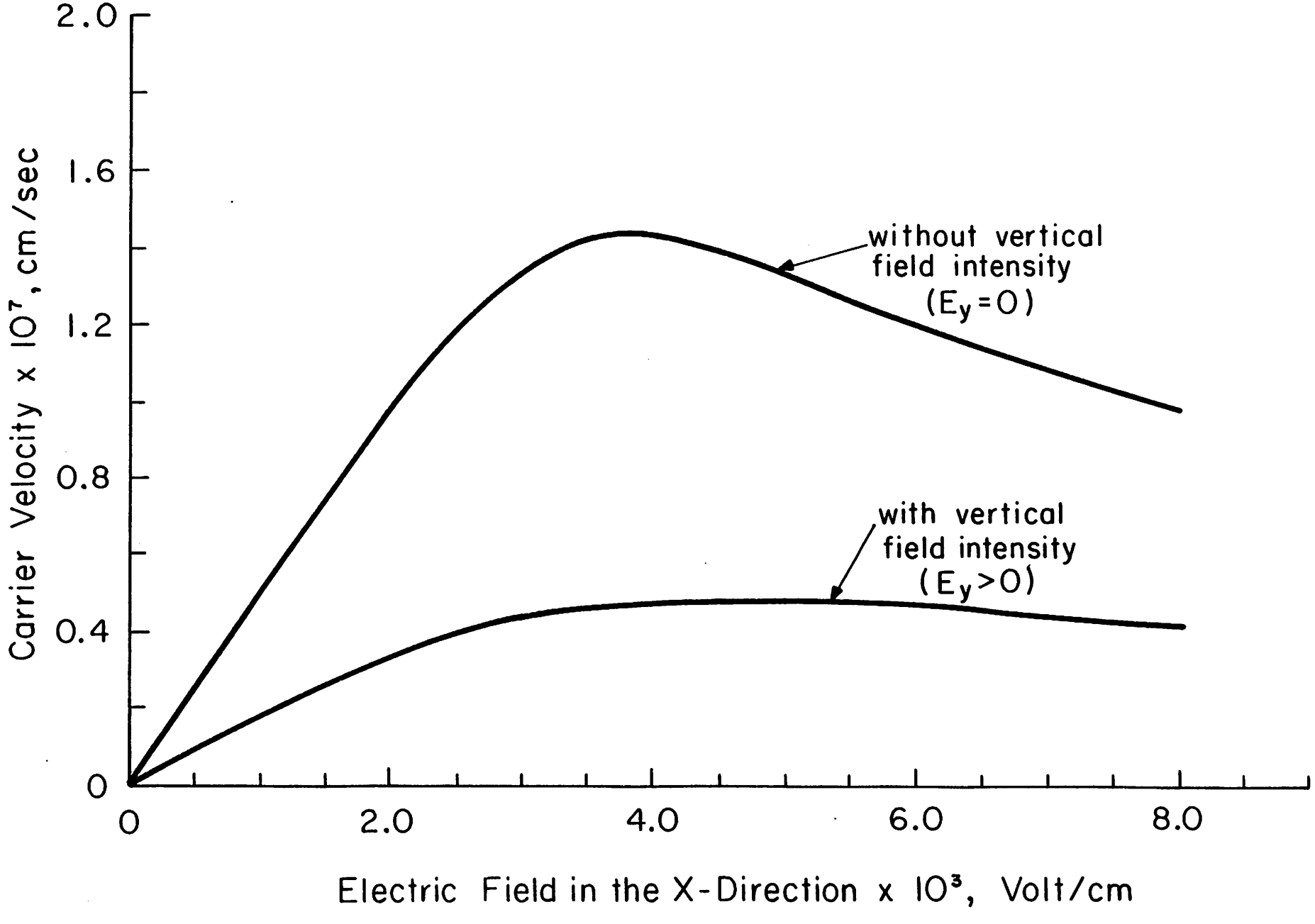
2.0
1.6
1.2
0.8
0.4
0
Carrier Velocity x $10^7$, cm/sec
without vertical field intensity ($E_y = 0$)
with vertical field intensity ($E_y > 0$)
0
2.0
4.0
6.0
8.0
Electric Field in the X-Direction x $10^3$, Volt/cm

Fig. 7